Solar Phys (2011) 272:137–157
DOI 10.1007/s11207-011-9811-9

Tracking a *Ulysses* High-latitude ICME Event Back to Its Solar Origins

C. Dumitrache · N.A. Popescu · A. Oncica

Received: 28 May 2010 / Accepted: 25 May 2011 / Published online: 21 July 2011

Abstract High-latitude interplanetary mass ejections (ICMEs) observed beyond 1 AU are not studied very often. They are useful for improving our understanding of the 3D heliosphere. As there are only few such events registered by the *Ulysses* spacecraft, the task of detecting their solar counterparts is a challenge, especially during high solar activity periods, because there are dozens coronal mass ejections (CMEs) registered by SOHO that might be chosen as candidates. We analyzed a high-latitude ICME registered by the *Ulysses* spacecraft on 18 January 2002. Our investigation focused on the correlation between various plasma parameters that allow the identification to be made of the ICME and its components such as the forward shock, the magnetic cloud and the reverse shock.

Using a linear approach and a graphical method we have been able to track the ICME event back to the Sun and to compute the day of the occurrence of the solar CME. In order to decide among several CME candidates which one is the right solar counterpart of our event, we have performed a follow-up computation of these CMEs from the Sun to *Ulysses*, by using two different speed formulas. First, the computation was simply based on the initial CME velocity, while the other was based on the ICME velocity estimated from the CME initial speed (Lindsay *et al.*, 1999). Differences of hours have been obtained between the arrival time predicted in these two ways, but the second one gave the best results. Both methods indicated the same two CMEs as the solar counterparts. We have found the solar source of these CMEs as being a huge polar filament that erupted in several steps.

This ICME event displayed a double magnetic cloud configuration. A minimum variance analysis helped us to detect the smooth rotation of the clouds and their helicity. Both magnetic clouds show the same helicity as the filament that erupted and released them. A cylinder-shape model of both clouds gives the same helicity sign.

C. Dumitrache (✉) · N.A. Popescu · A. Oncica
Astronomical Institute of Romanian Academy, 040557 Bucharest, Romania
e-mail: crisd@aira.astro.ro

N.A. Popescu
e-mail: nedelia@aira.astro.ro

A. Oncica
e-mail: adrian@aira.astro.ro

Keywords Coronal mass ejections · Interplanetary coronal mass ejections · Magnetic clouds · Prominences

1. Introduction

Coronal mass ejections (CMEs) are transient events that erupt into the interplanetary space. They are huge clouds of magnetized plasma traveling with velocities ranging from several hundreds to several thousands $\mathrm{km\,s^{-1}}$. Their signatures in the interplanetary space are different and their effects on space weather represent a keystone. Understanding the onset and the solar source of these phenomena, as well as their travel in space is a challenge since each event has its own particular characteristics. Dere and Balsubramanian (2001) analyzed the CMEs solar sources for 32 events and found that 59% of them originate from active regions without prominences and 22% are associated with eruptions of prominences embedded in active regions. Only 19% of CMEs originate from quiescent prominence eruptions.

It is generally known that the characteristics of the magnetic field at low and high latitudes are different, not least because of the solar activity features that manifest at those latitudes, active regions and polar filaments, respectively. Many CMEs originating at low latitudes could arrive at the Earth orbit at the ecliptic level. However, spacecraft flying near Earth cannot intercept those ICMEs occurring at high latitudes. Beyond 1 AU, the ICME identification is more difficult because some ICME signatures are blurred by the interaction with the ambient solar wind. Consequently, the observations provided by the *Ulysses* spacecraft during its transits over the solar poles are very important to help us understand how the high-latitude CMEs travel through space, far from the ecliptic and beyond 1 AU, and provide an insight to the 3D heliosphere.

Launched in October 1990, *Ulysses* was the first mission to explore the heliosphere from the solar equator to the poles. The results of data analysis reveal that the solar magnetic field is carried out in space in a more complicated manner than previously expected. The northern polar pass of *Ulysses* second orbit, in 2001, coincided with the phase of the solar cycle immediately following the sunspot maximum. After the Sun's polarity changed in 2001, huge filaments belonging to the polar crown developed and their eruption gave important CMEs. Gosling *et al.* (1994) first described the high-latitude class of ICMEs that were fully embedded within the polar fast streams. A forward-reverse shock pair is associated with these ICMEs; this is due to the over-expansion of the CME caused by internal pressure.

To track an ICME beyond 1 AU is not an easy task. One way to better understand how ICMEs evolve in the solar wind is to track specific ICMEs observed by spacecraft at different heliospheric distances. Wang, Du, and Richardson (2005) described the most important characteristics of ICMEs in the heliosphere between 0.3 and 5.4 AU, using data from several spacecraft. An excellent work has been done by Foullon *et al.* (2007) that investigated in detail a low latitude event coming from an active region filament and registered by more than one spacecraft. High-latitude ICMEs cannot be followed using observations by the *Advance Composition Explorer* (ACE), *Wind* or *Helios-1,* as the events are not located close to the ecliptic plane. Using data from *Ulysses* we have been able to track an event that occurred at high latitudes and far from Earth's orbit (1 AU), at times when the satellite passed over the solar poles. The latitude distribution of the CME occurrences is solar cycle dependent and this implies that only during some periods one can expect to observe high-latitude CMEs and ICMEs.

Many ICMEs include magnetic clouds (MCs) in their structure. A MC represents the interplanetary manifestation of a flux rope expelled from the Sun. Magnetic clouds were

defined by Klein and Burlaga (1981) as regions with a radial dimension of approximately 0.25 AU at 1 AU, in which the magnetic field strength is high. A smooth change of the field direction is observed when a spacecraft passes through the cloud. Combined with the low proton temperature, the strong magnetic field leads to a low proton β (proton to magnetic pressure ratio), $\beta < 2$.

As they propagate in the heliosphere, the CMEs' internal properties and configuration change as they expand, so it is difficult to relate back an ICME registered at several AUs. One parameter that can be measured *in situ* by satellites remains yet unchanged: this is the ionization level of the solar wind. By measuring the charge states of solar wind ions, thermodynamic properties present in the source region of the solar wind can be analyzed at any distances in the heliosphere. The charge states are higher inside most ICMEs, especially inside magnetic clouds. Rodriguez *et al.* (2004) extended Henke *et al.* (2001) the analysis to a set of 40 magnetic clouds detected by *Ulysses* and found that the increase of the charge state is present at all latitudes and phases of the solar cycle.

Many authors derived empirical models concerning CME propagation through the heliosphere from observational data. Lindsay *et al.* (1999) and Gopalswamy *et al.* (2001) developed simple shock arrival time models using the initial CME speed and ambient solar wind speed to predict the acceleration or deceleration of the CME. Gopalswamy *et al.* (2001) assumed that the CME speed matches the solar wind speed before 1 AU. Owens and Cargill (2004) analyzed the existing models of ICME travel times between Sun and Earth and found that all models had a similar accuracy for the predicted arrival time at 1 AU.

Neugebauer, Goldstein, and Goldstein (1997) discussed the radial field events that are defined as the events for which the condition $|B_r|/B > 0.9$ lasts for six hours or longer at 1 AU in the ecliptic plane. In a recent study, Du, Zuo, and Zhang (2010) found that about 43% of ICMEs were MCs and 23% were associated with radial events.

The track back to the Sun of an ICME registered at distances greater than 1 AU still remains a challenge. Several authors have identified the solar counterparts of *Ulysses*' ICMEs using different methods. We list here a few: energetic particle behavior observed by two spacecraft (Simnett, 2003), flux rope modeling (Watari, Watanabe, and Marubashi, 2002; Démoulin *et al.*, 2008), tracking the interplanetary scintillation close to the Sun and out of the ecliptic (Tokumaru *et al.*, 2006). Gazis *et al.* (2006) provided a list of works about *Ulysses*' ICMEs and their solar counterpart determination, but this list contains events that occurred until 2001. Another comprehensive work was done by van Driel-Gesztelyi and Culhane (2009) that synthesized the magnetic clouds characteristics and their relation to the solar sources.

In the present work we attempt to track back an ICME to its solar source by studying a high-latitude double event registered by SOHO and *Ulysses* satellites. We investigate the ICME registered by *Ulysses* on 18 January 2002. In Section 2, using the well-known MC signatures, we actually identify two MCs arriving successively at *Ulysses* and we analyse in detail the entire ICME limits. Tracking back of this double event to the Sun has indicated as solar source two CMEs in squall, registered by SOHO on 8 January 2002 and coming from a polar filament eruption. In Section 3 we propose a rough method to track back an ICME using a linear model. Using the CDAW CMEs catalogue (http://cdaw.gsfc.nasa.gov/CME_list) we select a few candidates for the solar counterparts of the studied ICME. Then, we follow these events from the Sun to *Ulysses* by computing the ICME arrival time using a linear model and two types of velocities. In Section 4 we describe the solar source of the two sequential CMEs we have found as the solar counterpart of the 18 January 2002 *Ulysses* event. The CMEs in squalls are defined as mass ejecta from the same solar source having decreasing velocities from one to the next (Dumitrache, 2009). In Section 5 we compute the MC

orientations and compare their topology to that of the erupting filament – their solar source. By applying the minimum variance analysis (MVA) we refine the MC limits, in order to obtain significant results. High-latitude ICMEs are limited to a very small number of observations and the task of solar counterpart detection is very complex. The event we study here belongs to the 21 ICME events and nine magnetic clouds registered by the *Ulysses* spacecraft in 2002 and listed by Du, Zuo, and Zhang (2010). These authors treated the ICME as a single MC. In this paper we have refined the analysis and shown that this event is in fact composed by two successive MCs coming from the same solar source and we established these MC limits. The computation of the MC axes was a challenge since their positions are far from the ecliptic plane and beyond 1 AU. The MVA gave statistically significant results and we show that these magnetic clouds did not merge, but they erupted from the Sun and traveled to *Ulysses* at slightly different latitudes. Our result contributes to the understanding of the high-latitudes CME traveling into the interplanetary space, far from the ecliptic plane and beyond 1 AU.

2. The ICME Characteristics

An ICME can be identified in the solar wind plasma by a combination of characteristics regarding its magnetic field, velocity, temperature and density. The ICME we have analyzed in this paper started on 18 January 2002, and lasted for 1.5 days according to Ebert *et al.* (2009). For its identification we have used observations provided by three instruments onboard of the *Ulysses* spacecraft, as follows. From SWOOPS we have used hourly averaged data of the solar wind plasma bulk parameters (i.e. velocity (v), proton density (N_p), proton temperature (T_p), alpha/proton abundance ratio ($N(\mathrm{He}^{++})/N(\mathrm{H}^{+})$). From VHM we have used also hourly data for the magnetic field magnitude (B), and components (B_r, B_t, B_n), given in RTN coordinates, where R is the axis in the direction from the Sun to the satellite, T is the cross product of the solar rotation axis and R, and N is the cross product of R and T. From SWICS we have used 3-hour averaged data for temperature, plasma composition and charge-state measurements of solar wind ions.

The interplanetary mass ejections are commonly identified by a set of signatures like (Richardson and Cane, 1993; Gazis *et al.*, 2006; Zurbuchen and Richardson, 2006):

- Alpha (He^{++}) abundance enhancement.
- Low ion temperatures during the event.
- Heavy ion species presenting anomalies of abundance and charge state.
- Bi-directional electron streaming, i.e. electrons moving in both directions along the magnetic field lines.
- Increased intensity of the magnetic field.
- Forward and reverse shocks when MCs are present.
- Smooth magnetic field rotation when MCs are present.

Figure 1 displays the evolution of the magnetic field magnitude (B) and the bulk plasma parameters – velocity (V), proton density (N_p), proton temperature (T_p), as well as alpha/proton ratio ($N(\mathrm{He}^{++})/N(\mathrm{H}^{+})$), for an interval of four days starting on 17 January 2002. The vertical lines mark the ICME limits that are expressed in days of the year and their fractions. By examining the magnetic field and velocity shape, but also the other ICME plasma signatures, as well as the MC topology determination using the minimum variance method (see Section 5), we propose the borders of the event as follows. We considered the whole event composed of two successive MCs for reasons we will discuss later in the paper.

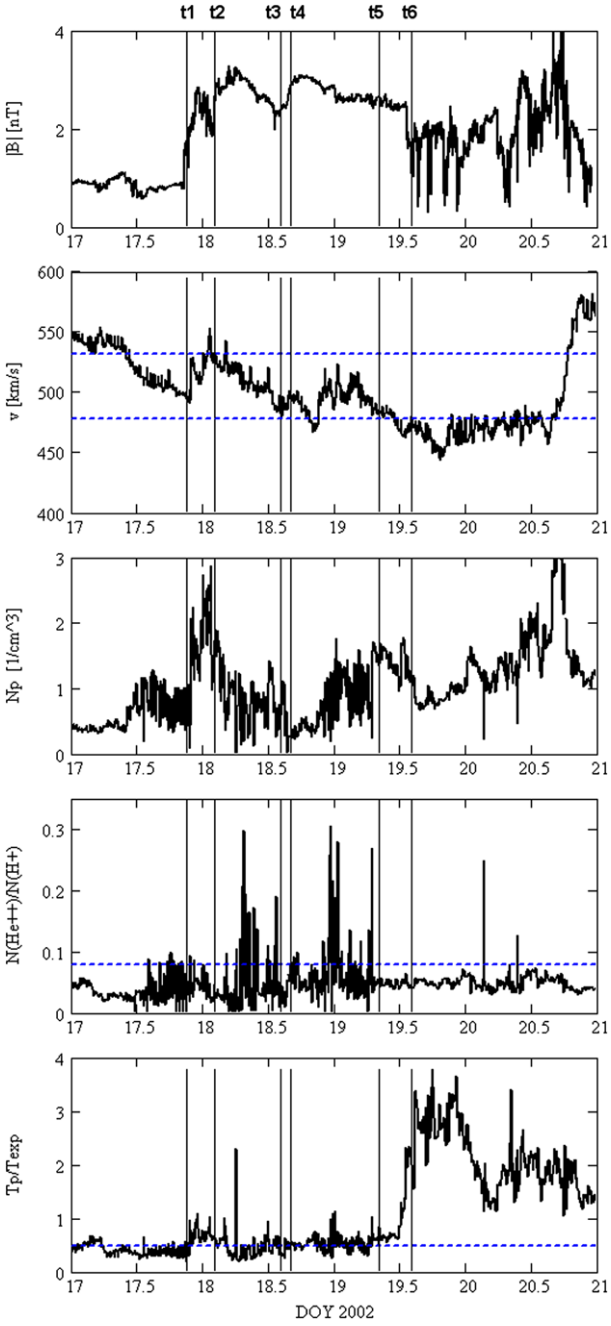

Figure 1 The magnetic field magnitude, velocity, proton density, alpha to proton density ratio, and T_p/T_{exp} temperatures ratio for an interval of four days between 17 – 20 January 2002 (VHM and SWOOPS instruments).

The forward shock started at $t1 = 17.875$ and the sheath developed until $t2 = 18.083$. The first MC (MC1) lasted from $t2 = 18.083$ to $t3 = 18.583$ and the second one (MC2) from $t4 = 18.667$ to $t5 = 19.333$. Using the proposed limits we have computed the radial widths of the MCs: 0.152 AU for MC1 and 0.19 AU for MC2. We notice that between $t2$ and $t5$

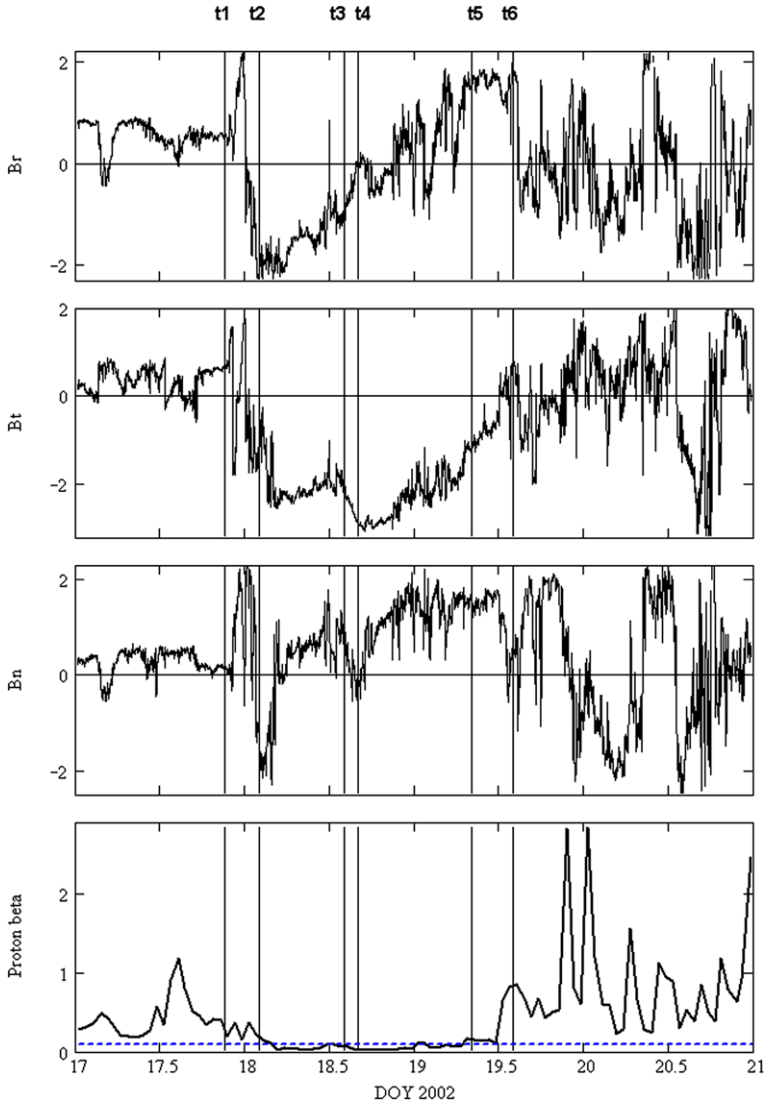

Figure 2 The magnetic field components B_{r}, B_{t}, B_{n} and the proton beta (VHM and SWOOPS instruments).

there are 0.41 AU as Du, Zuo, and Zhang (2010) found for this event. The reverse shock appeared at $t6 = 19.583$.

The presence of the forward shock in all magnetic field components (Figure 2) suggests a non-planar shock. We mention that the velocity reached a maximum 531.5 km s^{-1} before $t2$, at DOY $= 18.04$, and this is marked in Figure 1 with the horizontal superior dashed line plotted together with the velocity.

The He (alpha particles) abundance is considered by Von Steiger and Richardson (2006) the best signature to track an ICME in the heliosphere. An ICME is detected *in situ* by He abundance enhancement: the alpha particle density to H density should be greater than 0.08 (Neugebauer and Goldstein, 1997). We have used SWOOPS data to analyze the alpha

particle abundance enhancement. During the MC passage at *Ulysses* (between $t2$ and $t4$) we observe mainly two peaks of this quantity. Otherwise, a two-part shape of the entire event can be seen in all data, suggesting the presence of two successive MCs.

The low ion temperature, displayed in Figure 1 (bottom), represents a signature for MCs too (Richardson and Cane, 1993) and this happened during all the ICME between $t2$ to $t5$, i.e. a period of 30 hours. The ratio of the measured proton temperature to that of expected one for the normal solar wind (T_p/T_{exp}) represents a quantifiable ICME signature, where T_{exp} is calculated in 10^3 K units. This ratio should be less than 0.5. The expected temperature was computed for distances exceeding 1 AU (Wang, Du, and Richardson, 2005) to be

$$T_{exp} = \begin{cases} \frac{(0.031v-5.1)^2}{r^{0.7}}, & v < 500 \\ \frac{(0.51v-142)}{r^{0.7}}, & v \geq 500 \end{cases}$$

Interesting aspects can be inferred from the magnetic field components. The radial, tangential and normal components are plotted in Figure 2. From these we can see more easily the forward shock, the MC passages at *Ulysses* and the reverse shock.

Smooth magnetic field rotation is an *in situ* characteristic of MCs. This rotation will be discussed in detail in Section 5. In Section 4, we will discuss the solar source and we will see that actually there are two CMEs starting from the same solar filament. The fact of two CMEs occurring very close in time to one another is suggested by all plasma parameters plots, except for the plasma β, which remained smaller than 0.1 during the whole event, between $t2$ to $t4$.

During an ICME β significantly decreases, especially inside the MC. The proton β was computed using the formula: $\beta = p/(B^2/2\mu)$, where p, the proton pressure, is divided by the magnetic pressure. This parameter is displayed in Figure 2 (bottom) and its value indicates that the MC configuration is force free; $\beta < 0.1$ reveals the presence of solar coronal matter inside the MCs.

Elemental composition anomaly represents an important indicative of an *in situ* ICMEs presence. Burgi and Geiss (1986) stated that the charge-state information within an ICME reflects the temperature history of the solar counterpart. The charge-state composition of elements such as O, C, and Fe contains a coronal signature of the solar wind and extremely high charge states are associated with mass ejections. Very high charge states of Fe are considered the most reliable signature of an ICME (Lepri *et al.*, 2001). The Fe/O abundance ratio divided by the solar Fe/O ratio (about 0.05) represents a proxy for the strength of the first ionization potential fractionation. Weighted averages of all charge states from Fe(6+) to Fe(16+) are normally between 9 and 11 in the solar wind and higher values indicate the presence of an ICME (Lepri and Zurbuchen, 2004). Another signature of an ICME is to fulfill of the condition O(7+)/O(6+) > 1. In their study, Henke *et al.* (1998) asserted that an enhanced O(7+)/O(6+) density ratio is directly correlated with MCs.

From SWICS data we notice the presence of anomalies in ion abundances and charge states. The temperature values of different heavy ions are drawn by comparison in Figure 3. One observes that during the entire event, the temperatures of He(++), C(6+), O(6+) are low. The enhancement of C(6+), Ne(8+), Mg(10+) densities relative to O(6+) during the event are also displayed in Figure 3.

The charge-state values of Fe exceeding 11 reveal the presence of an ICME event and this happened in our case. The average iron charge state has values close to 15.5 at the first MC, almost reaching the maximum level that can be detected by SWICS (i.e. $\langle Q_{Fe} \rangle = 16$). Maybe this is the most reliable indicator of the presence of the ICME, and it correlates well with other charge states and element ratios (Figure 3).

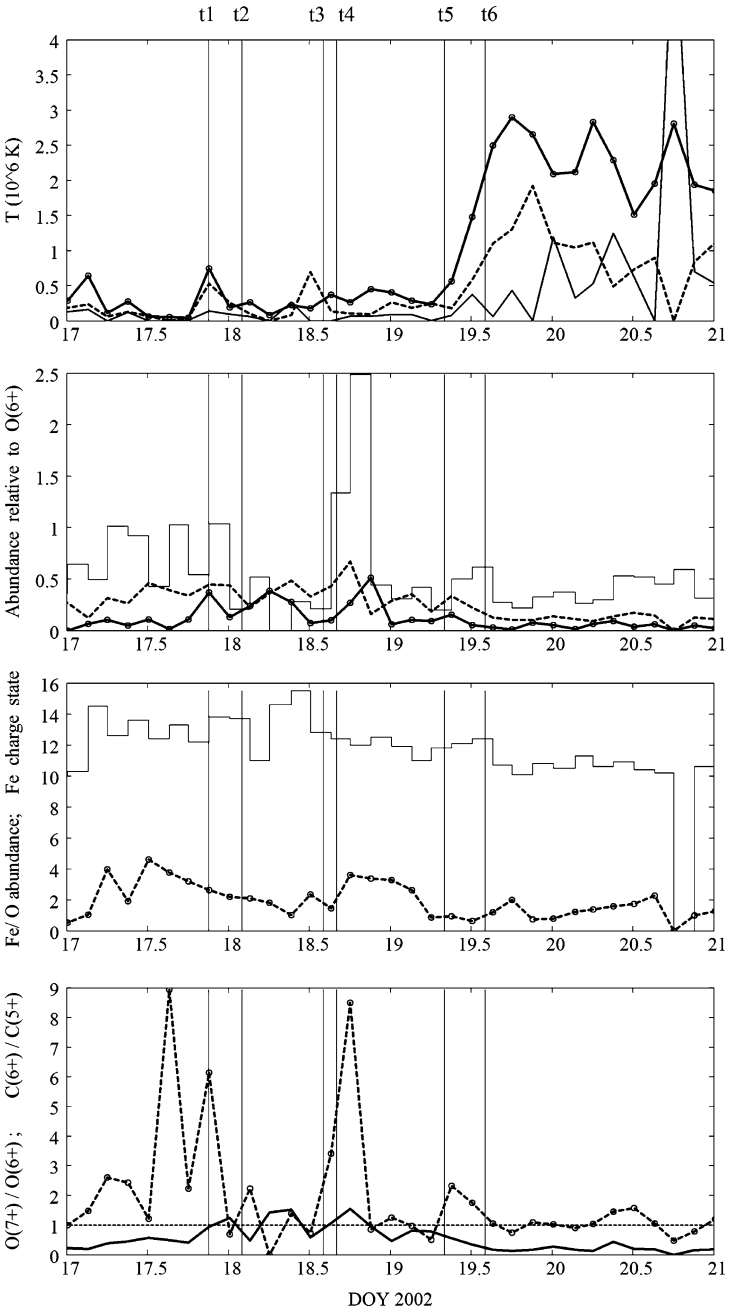

Figure 3 Top panel: the temperatures of different heavy ions: $T(\mathrm{He}^{++})$ – thin line, $T(\mathrm{C}^{6+})$ – dashed line, $T(\mathrm{O}^{6+})$ – thick line with circles. Second panel: the heavy ions' relative abundances: C(6+)/O(6+) – steps, Ne(8+)/O(6+) – dashed line, Mg(10+)/O(6+): thick line with circles. Third panel: Fe charge state (steps) and Fe/O ratio (dashed line with circles). Bottom panel: the C(6+)/C(5+) (dashed line with circles) and O(7+)/O(6+) (thick line) distributions. The horizontal dashed line represents the O(7+)/O(6+) = 1 condition. Data observed by *Ulysses* (SWICS instrument) are plotted for an interval of four days between 17 – 20 January 2002.

The Fe charge-state enhancements are commonly confined within the MC and correspond to the period of enhanced O(7+)/O(6+) density ratios, as can be seen in Figure 3 (third and bottom panels). The charge-state ratios, $C(6+)/C(5+)$ and O(7+)/O(6+), and their enhancement during this event are relevant too. The ionization ratio O(7+)/O(6+) ~ 1 corresponds to a coronal temperature of 2×10^6 °K. O(7+)/O(6+) = 1.5 coincides with the passage of the first MC, while during the passage of the second cloud, the C(6+)/C(5+) ratio reaches the value of 8.5 and O(7+)/O(6+) > 1 for an interval of almost six hours.

3. Tracking Back to the Sun

On 18 January 2002, *Ulysses* was situated at 2.7 AU and 62.18° north heliographic latitude relative to the Sun, after the solar pole overpass and SOHO–*Ulysses* quadrature in 2001. Figure 4 displays *Ulysses*' position on its orbit relative to the Sun and Earth (http://orbits.esa.int).

From *Ulysses*' mission we know that the spacecraft was at the following heliographic coordinates: 70° longitude and 64° latitude on 8 January 2002, and 68° longitude and 62° latitude on 18 January 2002. The Sun–Earth–*Ulysses* angle was 86.97° on 8 January and 89.85° on 18 January 2002. This *Ulysses* position allows the satellite to intercept mass ejected from the Sun under a certain position angle (PA) measured counter-clockwise from solar North in degrees (CDAW catalogue, http://cdaw.gsfc.nasa.gov/CME_list). A rough estimate of possible PAs inferred from the satellite's heliographic latitude gives values near 332°. A more exact estimation performed as Howard *et al.* (2007) or Webb *et al.* (2009) indicates a PA centered around 310°. In order to have a wide range to search we look for CMEs that occurred with a PA between 300° and 360°.

Using a linear approach for the motion law and a graphical method, we are able to track an ICME event back to the Sun and to compute the day of the occurrence of the solar counterpart, as a first approach. Figure 5 shows the DOYs of *Ulysses* observations on the vertical axis and the DOYs of the solar events on the horizontal axis. The hourly observations at *Ulysses* at tu_i are plotted versus $ts_i = doy_i - \mathrm{d}t_i$, where $\mathrm{d}t_i = s_i/v_i$ is the time period necessary for an event to travel from the Sun to the spacecraft with velocity v_i registered *in situ* and assumed to be constant from the Sun to *Ulysses*. The index i refers to the *Ulysses*

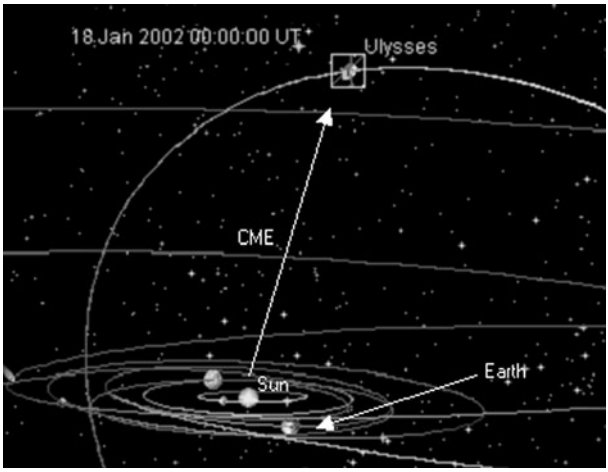

Figure 4 *Ulysses* spacecraft position relative to Sun and Earth, on 18 January 2002 (http://orbits.esa.int): one arrow points to Earth and the other indicates the Sun–*Ulysses* direction.

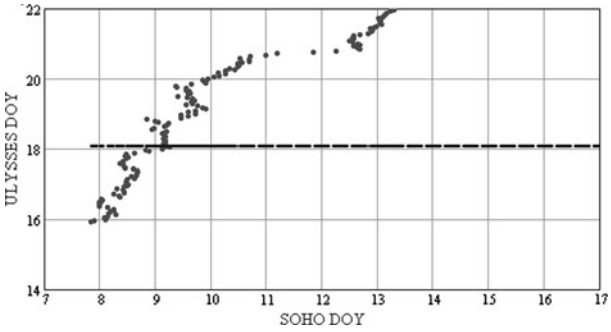

Figure 5 Diagram with DOYs of events registered by *Ulysses vs.* those that should be registered by SOHO.

Table 1 CME candidates to be the solar source of the ICME registered on 18 January 2002 by *Ulysses*. First six lines are extracted from the CDAW catalogue and the last position is derived from CACTus software.

No. crt.	Date	Time	PA	Linear speed	Our notation
1	07-01-2002	16:54:05	311	740	
2	08-01-2002	17:54:05	360	1794	
3	08-01-2002	18:30:05	345	566	CME1
4	08-01-2002	19:31:51	338	518	CME2
5	09-01-2002	18:54:05	351	113	
6	10-01-2002	05:54:05	301	403	
7	10-01-2002		309	589	CACTus

observations at time tu_i (hourly) and s_i is the corresponding distance between Sun and *Ulysses*. The dashed horizontal line marks $t2 = 18.083$, i.e. the DOY of the beginning of the analyzed ICME (first MC arrival). The intersection of the line with the points in Figure 5 indicates the day of the CME occurrence at the Sun, ts_i, which we read on the horizontal axis. We obtained 8 January 2002 as being the day of the CME occurrence and we search for it in SOHO data.

We have used the CMEs catalog from CDAW to identify the solar events registered by SOHO. We have searched for events around DOY $= 8 \pm 1$ and for events which occurred with PA greater than 300°, to have a wide-range search. Table 1 presents all these candidates. The last column contains our notation for the events that we inferred to be the solar counterparts of the analyzed ICME events, after this we have tracked from the Sun to *Ulysses* all CMEs listed in Table 1. One CME listed in Table 1 is a halo event. The last line of Table 1 contains the event detected by the CACTUS software (http://sidc.oma.be/cactus/). CACTUS detected the occurrence of a CME with a radial velocity 589 km s^{-1}, at PA = 309°, with an angular width equal to 18° on 8 January 2002.

Finally, we have to decide which one of the CME events was responsible for the interplanetary mass ejection registered by *Ulysses*. For that we used two models to compute the CME travel time through the interplanetary space.

First, we computed for each event listed in Table 1 the arrival time to *Ulysses* given by a linear model: $t_k = ts_k + v_{0k}$, where $k = 0, \ldots, 7$ refer to the seven events listed in Table 1, and the data ts_k and v_{0k} are provided by SOHO/LASCO spacecraft (CDAW catalogue). The arrival time prediction is plotted in Figure 6 with circles, where the horizontal line marks here the *Ulysses* event time on DOY = 18.083.

Gopalswamy (2002) derived an empirical model for the CMEs' travel in space and arrival time prediction. This model was designed for 1 AU and the ecliptic plane. By assuming

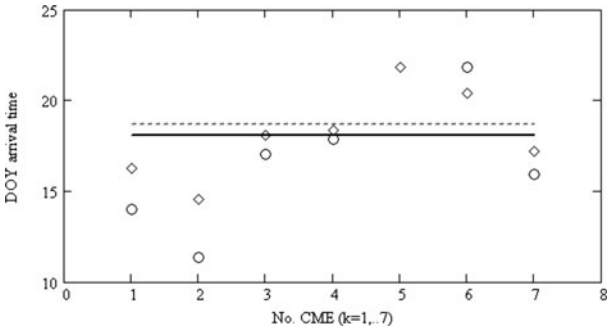

Figure 6 Diagram with the arrival time prediction of all events listed in Table 1, computed in two ways: with initial linear CME velocity (circles) and with Lindsay *et al.* (1999) velocity formula (diamonds). The horizontal lines represent the MC limits, $t2$ (solid line) and $t4$ (dashed line).

that the acceleration a depends linearly on the initial speed v_0, Gopalswamy (2002) fitted $a = 2.193 - 0.0054 \cdot v_0$. The distance after which $a = 0$ depends on both the CME speed and the background solar wind speed. Gopalswamy *et al.* (2001) estimated this distance to be about 0.76 AU. The interplanetary acceleration obtained above can be used in another kinematic relation, $v^2 = v_0^2 + 2a \cdot S$ to get the speed of the CME at a distance S, between the Sun and *Ulysses*, expressed in astronomical units. Same results as with the linear model are obtained using the Galileo formula and then $t_k = S/v_k$, where $S = 2.7$ AU in our case. Since a CME accelerates first and decelerates afterwards close to 1 AU, we could expect that globally for larger distances a CME has a linear velocity. Borgazzi *et al.* (2008) considered the ICME–solar wind interacting and the action of the laminar drag force and showed that this interaction produces within a few days the deceleration of the structure to an asymptotic value corresponding to the ambient solar wind velocity.

Lindsay *et al.* (1999) stated that CMEs observed at initial speeds below the average solar wind speed produce ICMEs accelerating, while CMEs with coronagraph speeds above the average solar wind speed produce ICMEs decelerating until they reach the ambient solar wind velocity. Lindsay *et al.* (1999) fitted a formula for the ICME speed v that depends on the initial speed v_0, using 49 events observed by *Helios-1* and *Pioneer Venus Orbiter* during quadrature periods with respect to the solar limb and the Earth.

We performed a second computation of the ICME travel times to *Ulysses* using the formula fitted by Lindsay *et al.* (1999), $v_k = v_{0k} \cdot 0.25 + 360$. In Figure 6 we plotted the results with circles for the first computation and with diamonds for the second one. The horizontal lines represent the MCs limits, $t2$ (solid line) and $t4$ (dashed line), respectively. Both computations of the ICME travel times described above, based on a linear model and different travel speeds, gave different results for the events listed in Table 1, but similar for both CME events we denoted as CME1 and CME2. The first method gives $t_{\mathrm{CME1}} = 17.02$ and $t_{\mathrm{CME2}} = 17.83$, while the second method gives $t_{\mathrm{CME1}} = 18.09$ and $t_{\mathrm{CME2}} = 18.36$. Consequently, we decided that these CME1 and CME2 events represent the solar counterparts of the successive magnetic clouds, MC1 and MC2, registered by *Ulysses* on 18 January 2002.

We have obtained two solar counterpart events and this result is consistent with the ICME signatures described in the previous section, where we have described a double high-latitude event. Both CMEs originated from the same solar source – a huge polar filament that erupted in several steps.

4. The Solar Source

The LASCO/C2 events registered at 18:30 UT (denoted here as CME1) and at 19:32 UT (CME2), coming from the same polar filament, are displayed in Figure 7. In Figure 8 we have plotted the convolutions of Hα images of the filament registered on 8 January 2002 at Big Bear Observatory. These convolutions reveal the CME onsets and the filament geometry and dynamics.

Dumitrache, Chifu, and Mierla (2008) have analyzed in detail the solar source that produced these explosive events. They are related to a filament observed on the solar disk between 3 and 8 January 2002. Three important parts composed this filament: the main (middle) body, a top, and a tail. These three components erupted at different moments, denoted with 1, 2 and 3 in Figure 9. CME1 represents the mass ejected from the main body of the filament, while CME2 corresponds to its top. The tail erupted few hours later and was not directed toward *Ulysses*. We have found that this filament destabilization is linked to the appearance and disappearance of two active regions situated more to the south, NOAA9765 and NOAA9766. Magnetic flux dispersion and new flux emergence produced a large-scale magnetic reconfiguration of the region that influenced directly the filament stability.

To get more information, we extrapolated the coronal magnetic field in 3D, using an IDL code developed by Lee, Gary, and Newman (2003). This code first detects several magnetic

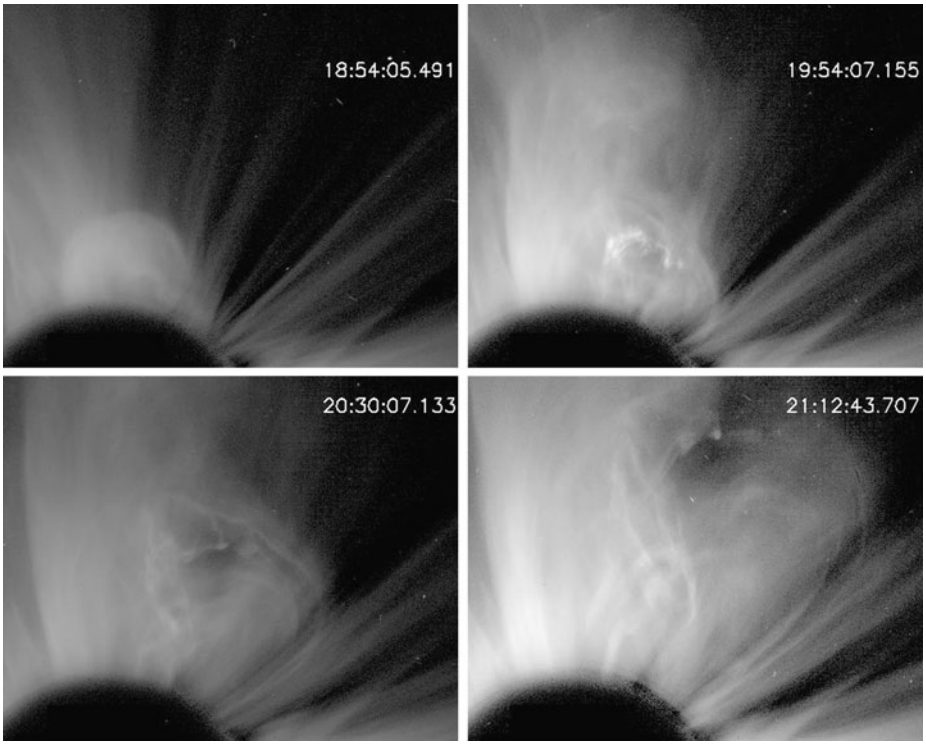

Figure 7 SOHO/LASCO C2 images of the coronal mass ejections.

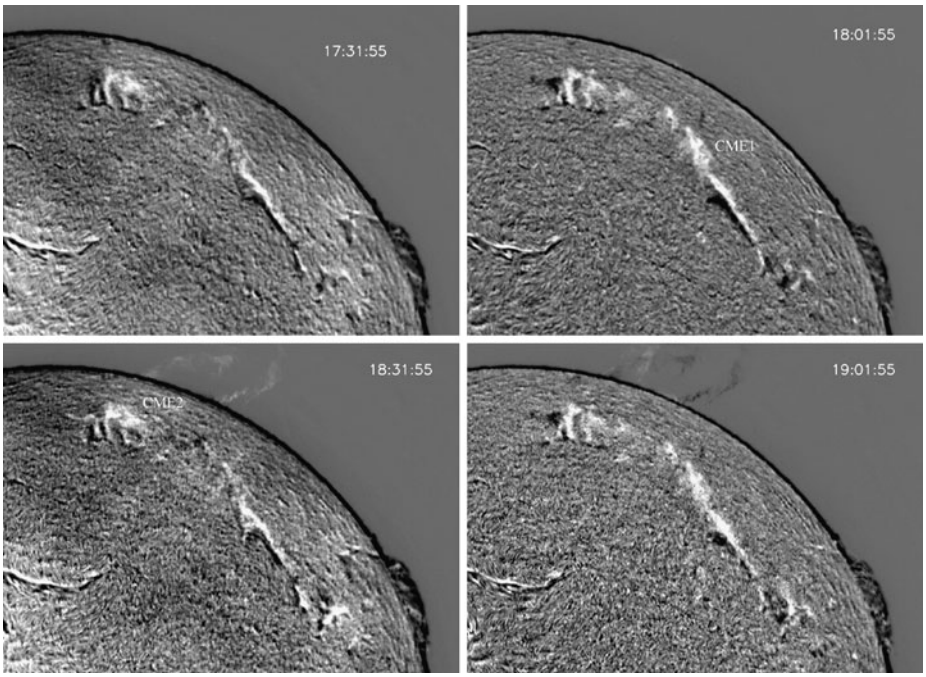

Figure 8 Convolutions of Hα images of the filament on 8 January 2002, obtained from Big Bear Observatory.

dipoles (we used ten dipoles) on the MDI magnetograms, in the zone of interest. Positions of these dipoles associated with the coronal image are obtained from the MDI magnetogram, in Cartesian coordinates. Finding the locations of dipoles from the magnetogram involves two steps:

i) Finding the xy coordinates of the major or dominant dipoles.
ii) Finding the z coordinates.

The xy coordinates of the positive polarity parts and of the negative polarity parts of the dipoles are found separately. These dipoles are located where B_z reaches a local extreme. The z coordinates of these dipoles are found using a technique that minimizes a function of two or more independent variables (Powell's method). Figure 9 displays the MDI magnetogram of the filament zone with all three erupting points of the filament (left panel) and the 3D extrapolated coronal magnetic field in the filament zone (right panel) at two moments – before and after the CME events occurred. Unfortunately, no magnetograms were available during the CMEs' onset. In Figure 9, we can see that the last erupting part of the filament, the tail corresponding to the third point, has very strong roots in the solar photosphere and for that reason was the most resistant to the perturbations coming from the neighbor active regions situated at the south. The last piece of the filament disappeared a few hours later, after 21:00 UT, around point 3. CME1 comes from the part that erupted in point 1 and CME2 comes from the top that erupted in point 2 of the filament.

In the EIT images we can observe that the filament lifts up in its middle part (point 1) and plasma is pushed toward its end points (points 2 and 3) starting at 15:36 UT. At 17:36 UT the rise of the middle part of the filament is easily visible. Some parts of the filament body

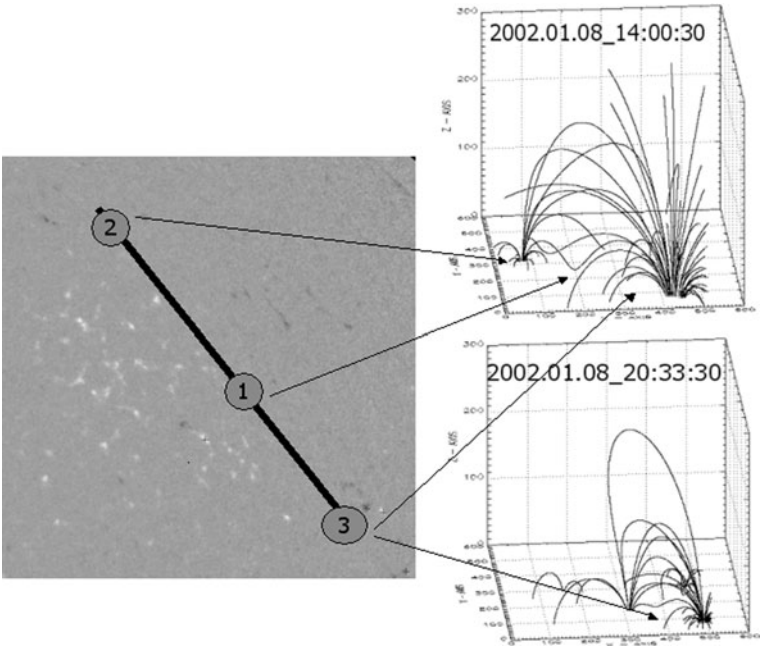

Figure 9 SOHO/MDI magnetogram and 3D coronal magnetic field lines extrapolated in the filament zone, before CME1 and after CME2.

broke at 17:12 UT and another at 18:12 UT. But the main phase of the mass ejections are at 18:24 UT (CME1) and then at 19:26 UT (CME2), when the flux ropes are ejected into space. Figure 10 displays few moments of this dynamics as registered by SOHO/EIT. The filament destabilization after local magnetic reconnections led to coronal mass ejections in squalls.

5. Orientation of the Magnetic Clouds

According to Burlaga (1988), the MCs are also characterized by a smooth coherent rotation of the magnetic field parallel to a plane when the spacecraft goes through the ICME considered as a flux rope. This rotation can occur in any direction on a time scale from few hours to days. We pursue to detect these changes of both magnetic cloud orientations in the Cartesian solar equatorial coordinates (X, Y, Z), where $B_x = -B_r$, $B_y = -B_t$, and $B_z = B_n$, *i.e.* B_y pointing to the East relative to the Sun. This implies that RTN coordinates are rotated by 180° around the normal axis (Mulligan and Russel, 2001). The directional changes of the magnetic field can be investigated with the minimum variance analysis (MVA) applied to the magnetic field components in these coordinates. Klein and Burlaga (1982) and Bothmer and Schwenn (1998) described in detail the MVA method applied to MCs.

We have calculated the covariance matrix M of the magnetic field components and its eigenvalues λ_k, with $k = 1, 2, 3$. By sorting the eigenvalues in decreasing order, the corresponding new directions are given by the eigenvectors $e_k = (x_k, y_k, z_k)$. The direction of the eigenvectors corresponding to the three axes (maximum, intermediate and minimum vari-

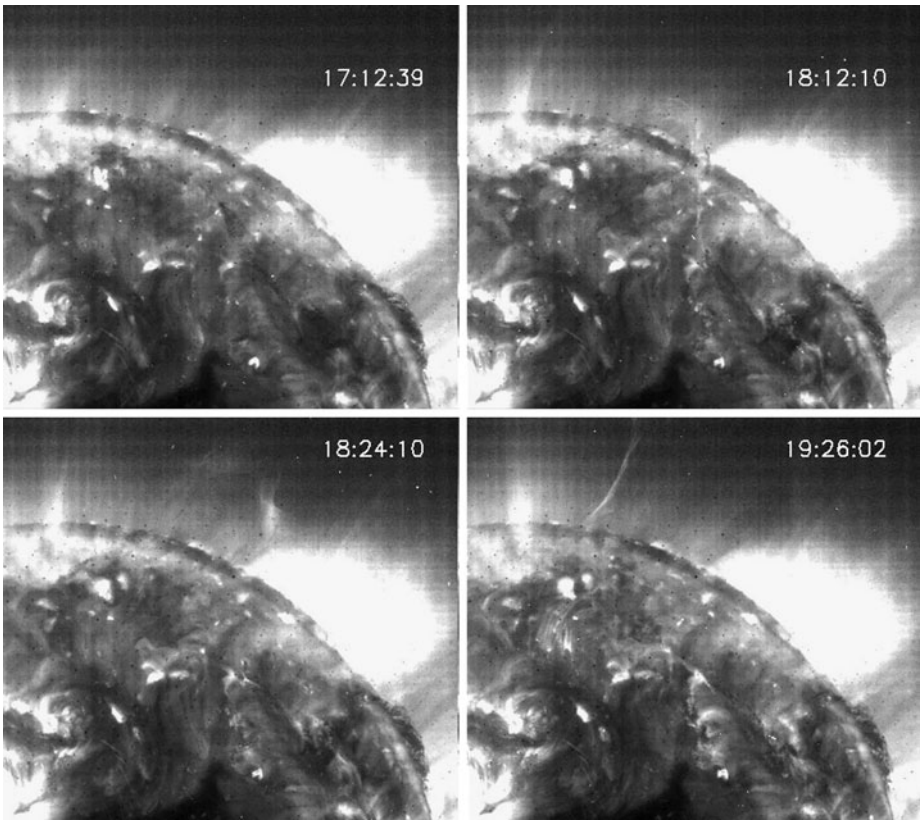

Figure 10 SOHO/EIT 195 Å images at different moments during the filament eruption.

ance) are given by

$$\varphi_k = \arctan(y_k/x_k)$$

$$\theta_k = \arctan\left(\frac{\sqrt{x_k^2 + y_k^2}}{z_k}\right)$$

where φ and θ are the azimuthal and elevation angles of the axis. We have obtained the magnetic field components of the clouds B_{xc}, B_{yc}, B_{zc} corresponding to the maximum variance, the intermediate and minimum variance directions, respectively. The method is relevant if $\lambda_2/\lambda_3 \geqslant 2$ and directional changes of the magnetic field vector exceed 30°. The OY_c new direction gives the orientation of the MC axis and we can detect a smooth coherent rotation in the X_cOY_c plane.

First, we performed the minimum variance analysis to the ICME as a whole, as previous authors did (Du, Zuo, and Zhang, 2010). We considered 1780 data registered between $t2$ to $t5$. The rate of λ_2/λ_3 gave 1.5. According to Lepping and Behannon (2001) this is a poorly determined case. In addition, the noise in the data was too high to be satisfactory.

Consequently, we applied the minimum variance analysis to MC1 from $t2$ to $t3$ and to MC2 from $t4$ to $t5$. In these time intervals there are 700 data points for MC1 and 900 for

Table 2 Magnetic cloud axis orientation obtained by minimum variance analysis, where θ and φ are the elevation angle and azimuthal angle, respectively, in RTN coordinates.

Cloud	Cloud axis		Min. var. dir.		λ_2/λ_3
	φ	θ	φ	θ	
MC1	227°	−90°	137°	66°	2.85
MC2	147°	38°	113°	58°	2.55

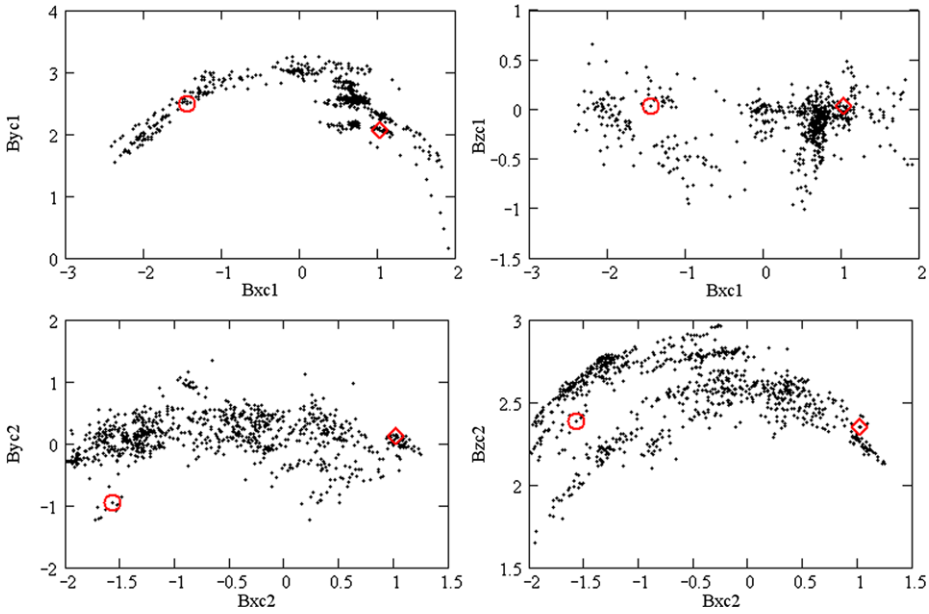

Figure 11 The rotations of the MCs computed with MVA in the intermediate–maximum variance plane (left) and in minimum–maximum variance plane (right). The circles indicate the start and the diamonds indicate the end for the sense of rotation.

MC2, in the VHM one-minute average data. With these cloud limits we obtained satisfactory results, listed in Table 2. Figure 11 displays these results; the rotation in the intermediate–maximum plane of variance (left panel) and minimum–maximum plane, respectively (right panel). The sense of rotation of the MCs is marked by the circle signs as starts, and by the diamonds as ends. We denoted by $(B_{xc1}, B_{yc1}, B_{zc1})$ the magnetic field vector for MC1 and with $(B_{xc2}, B_{yc2}, B_{zc2})$ for MC2, as obtained from the MVA computations. From the hodograms in Figure 11 we can deduce the magnetic cloud helicity signs (Bothmer and Schwenn, 1998). MC1 has a rotation in the Y_cOX_c plane in the negative sense (from circle to diamond) and the B_y values are positive. This field rotation implies that MC1 is left-handed and therefore the sign of its helicity is negative. The magnetic field variance in the X_cOZ_c plane is very small and we conclude that the MC1 orientation is well detected. For MC2, we have to deal with a not so clear situation. The rotation of the cloud in the X_cOY_c plane has also a negative sense, while the B_y magnetic field component values are in the vicinity of zero, with a positive predominance. For these reasons we assume that MC2 is also left-handed (negative helicity). The variance plot in the X_cOZ_c plane reveals a coherent rotation too. The eigenvalue ratios gave us significant results to validate the goodness of the orientations given by MVA. However, Gulisano *et al.* (2007) found that the MVA directions

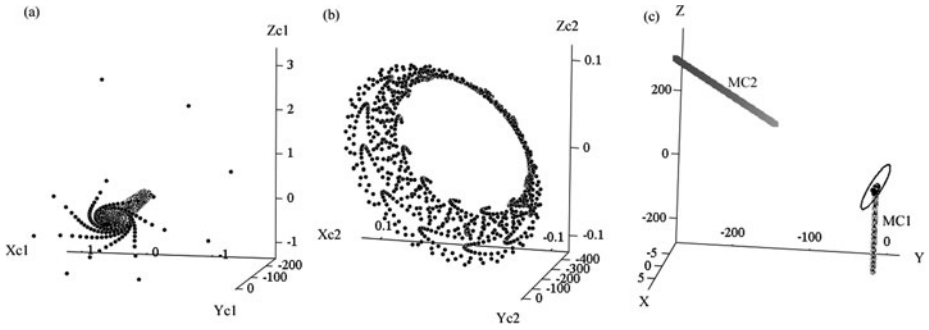

Figure 12 The magnetic clouds modeled as cylindric-shape flux tubes (a and b). The magnetic clouds relative positions, after their rotation (c). The ellipse marks the spacecraft.

can still deviate significantly from the main cloud axes, even when this criterion is very well satisfied. These authors pointed out the importance of the impact parameter, p, defined as the minimum distance from the spacecraft to the cloud axis. Estimation of the impact parameter p rated to the cloud radius gave us 0.156 for MC1 and 0.713 for MC2. Consequently, the spacecraft path was near the flux rope periphery of MC2 and the uncertainties associated with the orientation angles became very large. According to Gulisano *et al.* (2005) the large and coherent rotation cannot be easily distinguished in such case.

In order to detect the correct magnetic helicity, especially for MC2, we have computed the magnetic field lines using the cylinder-shaped flux rope model described by Marubashi and Lepping (2007). The cylindrical coordinates are (ρ, ψ, φ) and $B(t) = B_\varphi \cdot \widehat{e}_\varphi + B_\psi \cdot \widehat{e}_\psi$, where B_φ and B_ψ are computed using Bessel functions of the first kind of order 0 and 1. For both clouds we have taken a negative helicity for the B_φ expression. For each MC we have considered the force-free field parameter α so that $\alpha \cdot r = 2.4$ at the MC borders. The results are plotted in Figure 12 where each magnetic cloud is considered in its own system of coordinates. While the first magnetic cloud clearly reveals a left-handed magnetic helicity (Figure 12(a)), the second one has a very twisted magnetic field and a complex rotation at the *Ulysses* passage (Figure 12(b)).

To compare both clouds, we have computed the angle between the two normal axes to the respective planes $Y_c O X_c$ of MC1 and MC2; this angle is of 61°. We used Marubashi and Lepping (2007) method to bring the clouds to the same system of coordinates (X, Y, Z) for which we have applied the minimum variance computations. These results are presented in Figure 12(c), where the relative positions of MCs, after they have rotated, and also the ellipse which marks the spacecraft are displayed. This Figure gives us an idea about the angle made by the clouds with the spacecraft, as well as about the angle between MC1 and MC2. Démoulin (2008) presented a similar case with two successive MCs, where the second cloud is almost perpendicular to the first one.

Pevtsov and Balasubramaniam (2003) indicated that the Sun preferentially exhibits left-handed filaments in its northern hemisphere and right-handed in the southern one. Exceptions to this rule occur in up to 35% cases. The filament that erupted and gave both CMEs was observed in the northern hemisphere. The orientation of the erupting magnetic field configuration can be inferred directly from observations: MDI magnetogram (Figure 9 left), Hα filament (Figures 8 and 13), the coronal loops in EIT (Figure 10). Figure 13 synthesizes our knowledge about the solar source – the Hα filament (BBSO observations). The horizontal lines indicate the latitudes of the end foot-points of the middle part of the filament that gave CME1 and its top that gave CME2. Because the filament is a huge one, a difference

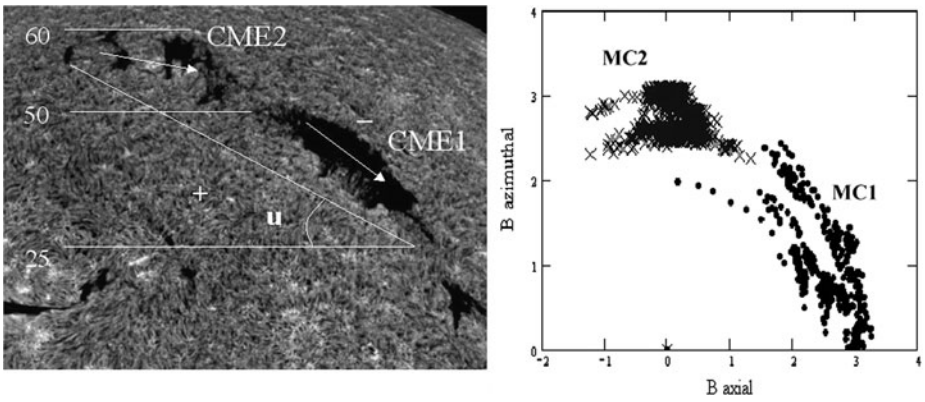

Figure 13 Left: The H_α filament with its two parts that erupted in CME1 and CME2. The filament barbs are well visible to infer the chirality. The filament respects the chirality rule of the northern hemisphere. Right: magnetic clouds plotted in cylindrical coordinates applied after MVA computations.

of almost 17 degrees exists between the mean latitudes of both filament parts implied in the eruptions. This figure displays the filament barbs clearly enough and we can see that the filament is dextral. This help us to infer the sense of the current in the filament channel. The arrows point to the sense of the current along parts of the filament axis. Plus and minus signs indicate the magnetic polarity from the MDI magnetogram (see also Figure 9). Another way to compute the filament helicity is presented by Dumitrache and Constantin (2010). This computation depends also on the filament tilt angle u made by the line between its end legs and the solar parallel (Figure 13 left). This computation gave also a negative helicity for the filament. With negative helicity and dextral chirality, this filament obeys the northern hemispheric rule.

Figure 13 (right) displays the magnetic field of MCs after MVA computations and also transformed to cylindrical coordinates. On our view the clouds have a similar shape and angle between them as the filament parts from where they originate. The azimuthal magnetic field is computed as $B_{pc} = \sqrt{B_{xc}^2 + B_{zc}^2}$, while the axial magnetic field is B_{yc}, for each MC.

MCs usually keep the same magnetic helicity as their solar source (Bothmer and Schwenn, 1998). But some MCs display a significant rotation of their axis compared to their associated filament. Green *et al.* (2007) analyzed seven cases of filament/MC associations having a large rotation, as we suspect is the case of MC2. They found that the direction of the rotation is related to the sign of the magnetic helicity as sign(rotation) $\cdot$ sign(helicity) > 0, with the rotation counted in the positive trigonometric sense from the filament to the MC axis direction. This condition is fulfilled by MC2; a negative sense of rotation and a negative helicity.

6. Conclusions

We summarize here the main results of our work. We have analyzed a high-latitude ICME registered by *Ulysses* spacecraft on 18 January 2002. We have used the signatures of He abundance enhancement, temperature depression, charge-state composition enhancement and low plasma β to identify the event from *in situ* measurements of the solar wind. All these signatures are present in this ICME; furthermore, a double MC structure is displayed.

We have inferred the MC boundaries from the magnetic field components and the velocity curve shapes. By applying a minimum variance analysis we have determined the MC orientations and the sense of their smooth rotations. All these computations indicated that both clouds have the same left-handed helicity as their solar source.

As the solar source of both CMEs we found a huge polar filament that erupted in many steps, producing sequential CMEr, or CMEs in squall. Large-scale magnetic reconnections caused by an emerging active region in the neighborhood produced the filament destabilization and the CMEs in squall.

The tracking of the event from 2.7 AU back to the Sun is not an easy task, since we have no additional information at 1 AU. We first considered a linear kinematic law to track the ICME back to the Sun using the velocity registered *in situ* by *Ulysses*. Therefore we introduced a graphic method to detect the day of the year when the event occurred on the Sun. We found several CME candidates to be the solar counterparts of the event registered by *Ulysses*. In order to distinguish which one is the right CME, we also track all CME candidates registered by SOHO until their arrival at *Ulysses*. This tracking was based on a linear model but using two different velocities: first, the initial linear CME velocities and, second, an empirical velocity formula that can be considered as the CMEs are embedded in the solar wind. Both computations indicated two CMEs as being responsible for the double MC event registered by *Ulysses* on 18 January 2002.

The errors given by the arrival times estimated in Section 3 and related to the moment $t2$ ($t_{\text{arrival}} - t2$) are the following:

- The first method gives -25.42 hours for CME1 and -6.03 hours for CME2.
- The second method gives 0.05 hours for CME1 and 6.56 hours for CME2.

By relating the second CME to $t4$ we obtained -20 hours error with the first computation and -7.4 hours with the second one.

We recall that CME1 left the Sun with a linear speed of 566 km s^{-1} and CME2 with 518 km s^{-1}. The erupting filament position on the solar disk was close to the western limb, this means the radial velocities of both CMEs do not differ too much from the measured ones. The event we analyzed in this work is observed when *Ulysses* and SOHO were almost in quadrature and the solar source is relatively close to the western solar limb. This configuration permits the observation in the plane of the sky from the coronagraph field of view. We remark that the solar source is almost near the western solar limb and therefore the radial velocity is not far from the projected velocity onto the sky, estimated from LASCO. As Démoulin (2008) showed, the observations in quadrature permit to detect the bright core in the CME center. This fact is visible in Figure 7, especially for the first CME (at 19:54 UT).

The CMEs in squalls that we found to be the solar counterparts of a high-latitude double ICME registered by *Ulysses* have moderate velocity values, little higher than 500 km s^{-1}. In their way from the Sun to *Ulysses* (2.7 AU), both CMEs have slowed down: the first CME velocity decreased by 41.5 km s^{-1} and the second one by almost 25 km s^{-1}.

Both MCs we have analyzed display a left-handed helicity, similar to the filament helicity. We have also modeled the clouds as cylinder-shape flux ropes and investigated their shape and helicity. But MC2 appears to be very twisted and has a double rotation at the spacecraft encounter: around its axis, but also around its OZ axis. The same left-handed helicity can be observed at their solar source represented by a huge polar filament with several parts. The filament respects the chirality rule of the northern hemisphere.

Each CME has a unique evolution and the forecast of the ICME arrival time at a certain distance in the heliosphere may raise different questions. This pair of events (8/18 January

2002) helped us to better understand aspects of the CME travels and space weather conditions at high latitudes and beyond 1 AU.

Acknowledgements This research was carried out under the ESA-PECS Contract C98055. SOHO and *Ulysses* are projects of international cooperation between ESA and NASA. The CME catalog is generated and maintained at the CDAW Data Center by NASA and The Catholic University of America in cooperation with the Naval Research Laboratory.

We thank the referee and the editors for the useful remarks that have helped us to improve the manuscript.

References

Borgazzi, A., Lara, A., Romero-Salazar, L., Ventura, A.: 2008, *Geofís. Int.* **47**, 301.
Bothmer, V., Schwenn, R.: 1998, *Ann. Geophys.* **16**, 1.
Burgi, A., Geiss, J.: 1986, *Solar Phys.* **103**, 347.
Burlaga, L.F.: 1988, *J. Geophys. Res.* **93**, 7217.
Démoulin, P.: 2008, *Ann. Geophys.* **26**, 3113.
Démoulin, P., Nakwacki, M.S., Dasso, S., Mandrini, C.H.: 2008, *Solar Phys.* **250**, 347.
Dere, K.P., Balsubramanian, S.: 2001, In: *Recent Insights into the Physics of the Sun and Heliosphere: Highlights from SOHO and Other Space Missions*, *Proc. IAU Symp.* **203**, 362.
Du, D., Zuo, P.B., Zhang, X.X.: 2010, *Solar Phys.* **262**, 171.
Dumitrache, C.: 2009, *Universal Heliophysical Processes*, *IAU Symp* **257**, 251.
Dumitrache, C., Constantin, D.: 2010, *Rom. Astron. J.* **20**, 35.
Dumitrache, C., Chifu, I., Mierla, M.: 2008, *Rom. Astron. J. Suppl.* **18**, 201.
Ebert, R.W., McComas, D.J., Elliott, H.A., Forsyth, R.J., Gosling, J.T.: 2009, *J. Geophys. Res.* **114**, A01109.
Foullon, C., Owen, C.J., Dasso, S., Green, L.M., Dandouras, I., Elliott, H.A., Fazakerley, A.N., Bogdanova, Y.V., Crooker, N.U.: 2007, *Solar Phys.* **244**, 139.
Gazis, P.R., Balogh, A., Dalla, S., Decker, R., Heber, B., Horbury, T., Kilchenmann, A., Kota, J., Kucharek, H., Kunow, H., Lario, D., Potgieter, M.S., Richardson, J.D., Riley, P., Rodriguez, L., Siscoe, G., von Steiger, R.: 2006, *Space Sci. Rev.* **123**(1 – 3), 417.
Gopalswamy, N.: 2002, *Solar-Terrestrial Magnetic Activity and Space Environment*, 157.
Gopalswamy, N., Lara, A., Yashiro, S., Kaiser, M.L., Howard, R.A.: 2001, *J. Geophys. Res.* **106**, 29207.
Gosling, J.T., McComas, D.J., Phillips, J.L., Weiss, L.A., Pizzo, V.J., Goldstein, B.E., Forsyth, R.: 1994, *Geophys. Res. Lett.* **21**, 2271.
Green, L.M., Kliem, B., Török, T., van Driel-Gesztelyi, L., Attrill, G.D.R.: 2007, *Solar Phys.* **246**, 365.
Gulisano, A.M., Dasso, S., Mandrini, C.H., Démoulin, P.: 2005, In: Fleck, B., Zurbuchen, T.H., Lacoste, H. (eds.) *Solar Wind 11/SOHO 16, Connecting Sun and Heliosphere* **SP-592**, ESA, Noordwijk, 621.
Gulisano, A.M., Dasso, S., Mandrini, C.H., Démoulin, P.: 2007, *Adv. Space Res.* **40**, 1881.
Henke, T., Woch, J., Mall, U., Livi, S., Wilken, B., Schwenn, R., Gloeckler, G., von Steiger, R., Forsyth, R.J., Balogh, A.: 1998, *Geophys. Res. Lett.* **25**, 3464.
Henke, T., Woch, J., Schwenn, R., Mall, U., Gloeckler, G., von Steiger, R., Forsyth, R., Balogh, A.: 2001, *J. Geophys. Res.* **106**, 10597.
Howard, T.A., Fry, C.D., Johnston, J.C., Webb, D.F.: 2007, *Astrophys. J.* **667**, 610.
Klein, L.W., Burlaga, L.F.: 1981, *NASA STI/Recon Tech. Rep. N* **81**, 28394.
Klein, L.W., Burlaga, L.F.: 1982, *J. Geophys. Res.* **87**, 613.
Lee, J.K., Gary, G.A., Newman, T.S.: 2003, *Bull. Am. Astron. Soc.* **35**, 809.
Lepping, R.P., Behannon, K.W.: 2001, *J. Geophys. Res.* **85**(A9), 4695.
Lepri, S.T., Zurbuchen, T.H.: 2004, *J. Geophys. Res.* **109**(A6), 2312.
Lepri, S.T., Zurbuchen, T.H., Fisk, L.A., Richardson, I.G., Cane, H.V., Gloeckler, G.: 2001, *J. Geophys. Res.* **106**, 29231.
Lindsay, G.M., Luhman, J.G., Russell, C.M., Gosling, J.T.: 1999, *J. Geophys. Res.* **104**, 12515.
Marubashi, K., Lepping, R.P.: 2007, *Ann. Geophys.* **25**, 2453.
Mulligan, T., Russel, C.T.: 2001, *J. Geophys. Res.* **106**, 10581.
Neugebauer, M., Goldstein, R.: 1997, *Geophys. Monogr.* **99**, 245.
Neugebauer, M., Goldstein, R., Goldstein, B.E.: 1997, *J. Geophys. Res.* **102**, 19743.
Owens, M., Cargill, P.: 2004, *Ann. Geophys.* **22**, 661.
Pevtsov, A.A., Balasubramaniam, K.S.: 2003, *Adv. Space Res.* **32**, 1867.
Richardson, I.G., Cane, H.V.: 1993, *J. Geophys. Res.* **98**, 15295.
Rodriguez, L., Woch, J., Krupp, N., Fränz, M., von Steiger, R., Forsyth, R., Reisenfeld, D., Glameier, K.-H.: 2004, *J. Geophys. Res.* **109**, A01108.

Simnett, G.M.: 2003, *Solar Phys.* **213**, 387.
Tokumaru, M., Kojima, M., Fujiki, K., Yamashita, M.: 2006, *Nonlinear Process. Geophys.* **13**, 329.
van Driel-Gesztelyi, L., Culhane, J.L.: 2009, *Space Sci. Rev.* **144**, 351.
Von Steiger, R., Richardson, J.D.: 2006, *Space Sci. Rev.* **123**, 111.
Wang, C., Du, D., Richardson, J.D.: 2005, *J. Geophys. Res.* **110**, 10107.
Watari, S., Watanabe, T., Marubashi, K.: 2002, *Adv. Space Res.* **29**, 451.
Webb, D.F., Howard, T.A., Fry, C.D., Kuchar, T.A., Odstrcil, D., Jackson, B.V., Bisi, M.M., Harrison, R.A., Morrill, J.S., Howard, R.A., Johnston, J.C.: 2009, *Solar Phys.* **256**, 239.
Zurbuchen, T.H., Richardson, I.G.: 2006, *Space Sci. Rev.* **123**, 31.